Flexible InGaAs Photodetector With High-Speed Detection and Long-Term Stability

Yuting Ye , Hui Ma , Jianghong Wu , Boshu Sun , Jialing Jian , Maoliang Wei , Renjie Tang , Yilin Shi , Hongtao Lin , *Member, IEEE*, and Lan Li *, Member, IEEE*

(Invited Paper)

Abstract—**Flexible photodetectors have garnered extensive research interest due to their potential applications in optical communications, sensing, and wearable systems. However, their operating frequencies have been limited to less than 10 MHz, which falls significantly below the requirements for certain applications. Here, we present a high-performance flexible photodetector based on InGaAs nanomembrane fabricated on a flexible plastic foil, where epitaxial layers are bonded with adhesives before being lifted from the parent InP substrate via a simple wet etching step. No mechanical polishing is involved, reducing the complexity of the fabrication procedure. The flexible photodetector exhibits impressive characteristics, including a low dark current of 801 pA, a responsivity of 0.51 A/W, a high detectivity of 5.65×10^{10} Jones, and a linear dynamic range over 70 dB at an applied voltage of 6 V in 1550 nm. Furthermore, we have prioritized efficient and high-speed collection of photogenerated carriers by optimizing the design of interdigitated detection electrodes. Dynamic measurements indicate that the photodetector surpasses a 3-dB bandwidth of 2.03 GHz, enabling it to support a data communication rate of 4 Gb/s. Additionally, this flexible photodetector demonstrates a wide operational wavelength range, covering nearly the entire telecom band from 1260 nm to 1620 nm, in both its planar state and half-cylindrically curved shape. More importantly, the obtained photodetector maintains high performance with long-term thermal and mechanical stability, holding great potential for developing advanced high-speed optoelectronics in wearable devices.**

Index Terms—**Flexible photodetectors, high-speed detection, InGaAs nanomembrane, optical communication, long-term stability.**

Yuting Ye is with the State Key Laboratory of Modern Optical Instrumentation, College of Information Science and Electronic Engineering, Zhejiang University, Hangzhou 310027, China, also with the Key Laboratory of 3D Micro/Nano Fabrication and Characterization of Zhejiang Province, School of Engineering, Westlake University, Hangzhou 310030, China, and also with the Institute of Advanced Technology, Westlake Institute for Advanced Study, Hangzhou 310024, China (e-mail: yeyuting@westlake.edu.cn).

Hui Ma, Maoliang Wei, and Hongtao Lin are with the State Key Laboratory of Modern Optical Instrumentation, College of Information Science and Electronic Engineering, Zhejiang University, Hangzhou 310027, China (e-mail: atticusmhh@zju.edu.cn; ml_wei@zju.edu.cn; hometown@zju.edu.cn).

Jianghong Wu, Boshu Sun, Jialing Jian, Renjie Tang, Yilin Shi, and Lan Li are with the Key Laboratory of 3D Micro/Nano Fabrication and Characterization of Zhejiang Province, School of Engineering, Westlake University, Hangzhou 310030, China, and also with the Institute of Advanced Technology, Westlake Institute for Advanced Study, Hangzhou 310024, China (e-mail: wujianghong@westlake.edu.cn; sunboshu@westlake.edu.cn; jianjialing@westlake.edu.cn; tangrenjie@westlake.edu.cn; shiyilin@westlake.edu.cn; lilan@westlake.edu.cn).

Color versions of one or more figures in this article are available at https://doi.org/10.1109/JSTQE.2024.3350431.

Digital Object Identifier 10.1109/JSTQE.2024.3350431

I. INTRODUCTION

IN the era of ubiquitous computing and the Internet of Things (IoT), there is a growing demand for high-speed optical data acquisition in various applications, including communication systems [1], [2], [3], [4], [5], wearable devices [6], [7], [8], and optical interconnect [9], [10]. Photodetectors (PDs) play a pivotal role in converting optical signals into electrical signals, making them critical components in these systems. Additionally, the development of conformable and wearable photodetectors is necessary to address communication requirements in complex environments [11], [12], [13], [14], [15]. Flexible photodetectors offer several advantages over their rigid counterparts, including conformal contact with curved surfaces, enhanced wearability, and compatibility with unconventional form factors. However, to meet the demands of these applications, the flexible photodetector must maintain the long-term stability of materials and structures while collecting photogenerated charge carriers efficiently and quickly. The technology for optimizing flexible photodetectors is still in the exploratory stage of developing various flexible photo-active films. Till now, diverse material platforms, including organic semiconductors [16], [17], [18], [19], [20], perovskites [21], [22], [23], [24], [25], two-dimensional materials [26], [27], [28], [29], [30], [31], nanowires or nanotubes [32], [33], [34], [35], [36], quantum dots [37], [38], [39], [40], [41], [42], and semiconductors nanomembranes (NMs) [43], [44], [45], [46], [47], [48], have been applied for fabricating flexible photodetectors with different device performance. For instance, although organic semiconductors and perovskite thin films have excellent flexibility, they suffer from poor thermal stability and low electron transport and collection efficiency. Two-dimensional materials, with only single-layer or few-layer structures, have low light absorption efficiency. Single nanowires have good mechanical performance, but using nanowire networks sacrifices the transport performance of

photogenerated carriers. Above all, it is evident that these new materials have inherent defects in device stability and response speed, rendering them unsuitable for developing high-speed flexible photodetection devices.

Semiconductor materials exhibit exceptional optoelectronic properties and have been widely applied in developing high-speed photodetectors. The transfer of semiconductor nanomembrane for high-performance flexible photodetectors is currently a prominent area of research in optoelectronics. Various types of semiconductor-based free-space flexible detectors have been reported in recent years. Silicon NMs (Si NMs) have been stacked and transferred on glass, polyimide (PI), and various other foreign substrates [49], [50]. Germanium (Ge) photodetectors with flexible structures have also been reported [51], [52], [53], but so far, due to their inferior mechanical flexibility, the realized flexible Ge PDs have only demonstrated limited performance. Additionally, NMs based on III-V materials with desired electronic and photonic properties have also been developed for heterogeneous integrated circuits [48]. Direct-bandgap semiconductor InP and its lattice-matched compound semiconductors (GaInAsP, GaInAlAs) are considered for fabricating high-performance optoelectronic devices in the short-wave infrared (SWIR) band. However, due to the limitations in physics, processes, and the mechanical properties of basic optoelectronic components, there remain only a few reports on semiconductor-based flexible free-space high-speed photodetectors, where the response speed of these photodetectors has not exceeded 10 MHz. It should be noted that key issues such as the fabrication of high-quality, low-defect nanomembranes, efficient collection of photogenerated carriers, and elimination of bending stress have not yet been resolved. The lattice-matched III-V ternary composite, $In_{0.53}Ga_{0.47}As$ (InGaAs), is a relevant material with an absorption constant of 7000 cm^{-1} at 1550 nm [54]. Electron and hole saturation drift velocities play a crucial role in determining the speed of the photodetector. For InGaAs, reported values of 6.5×10^6 cm/s and 4.8×10^6 cm/s have been documented for electrons and holes, respectively [55]. In addition, the thickness of the InGaAs absorber layer can be precisely controlled through epitaxial growth and lifted off from the InP substrate using wet etchants with a high selectivity ratio. Therefore, InGaAs emerges as a robust candidate material for high-speed photodetectors.

Here, we demonstrate flexible photodetectors based on In-GaAs (Epihouse Optoelectronics Co., Ltd.) NMs fabricated on a flexible substrate. The fabrication process involves adhesives to bond epitaxial layers, which are then separated from the parent InP substrate solely through wet chemical etching. This approach ensures the retention of exceptional device performance while simplifying the manufacturing process. The obtained photodetectors exhibit outstanding performance in terms of detectivity, response speed, and linear dynamic range while also demonstrating remarkable mechanical flexibility and long-term stability. These achievements advance our understanding of flexible photodetector technology and provide valuable insights for the practical development of cutting-edge wearable applications that require rapid optical data acquisition, such as health
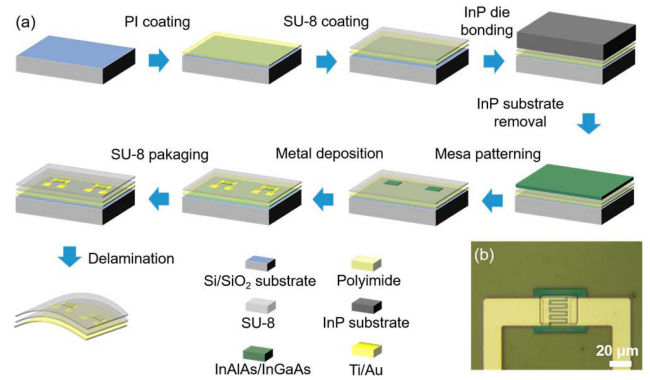

Fig. 1. (a) Flow chart for flexible InGaAs photodetector preparation process; (b) Top-view optical microscope graph of the fabricated flexible InGaAs photodetector.

monitoring sensors [56], [57], [58], [59], image sensors [60], [61], [62], [63], [64], and optical communications [65], [66].

II. DEVICE FABRICATION

The fabrication process flow of the flexible InGaAs photodetector is schematically illustrated in Fig. 1(a). Initially, a PI film was spin-coated onto a 500 nm oxide-coated silicon wafer, serving as the handle substrate. Simultaneously, the InP die (5 mm × 5 mm) cap layer was selectively etched out by wet etching in a H_3PO_4/HCl (7:3) solution for 1 minute over the InGaAs absorption layer. Next, an adhesive agent, SU-8 epoxy film (Microchem, SU-8 2002), was spin-coated onto the top of the PI film and subsequently soft-baked at 95 °C for 1 minute. To enhance the adhesion of device bonding, the SU-8 film underwent exposure at half the recommended dose suggested by the manufacturer, leading to partial epoxy cross-linking. Then the InP die was subsequently bonded onto the handle wafer, ensuring that the InGaAs absorption layer was facing the SU-8 epoxy. The custom-built pressure loader facilitated the bonding process. The process was conducted in a vacuum oven at a temperature of 90 °C for 20 minutes, followed by a temperature of 150 °C for 30 minutes. Afterward, the sample and the loader were cooled to room temperature to prevent any potential cracking of the epi-layer. The InP substrate was removed using the wet chemical etching process, leaving behind the NM structure. This structure consists of an InGaAs absorber layer, an InAlAs Schottky barrier enhancement layer (SBEL), and a lattice matching layer sandwiched between them. The composite epitaxial layer for the InGaAs/InAlAs MSM detector has a total thickness of approximately 205 nm. Table I contains information about the complex epitaxial layer. After removing the substrate, photolithography techniques were used to pattern the InGaAs NM and define the photodetector mesas. Detailed processing parameters of the InGaAs NM wet etching steps can be found in our previous study [67]. Compared to prior studies, we have streamlined the preparation process, eliminating the complex and time-consuming mechanical polishing step. Instead, the InP substrate was directly removed through wet

TABLE I
EPITAXIAL LAYER STRUCTURE OF THE INGAAS/INALAS MSM DETECTOR

| Material	Thickness (nm)	Function
i-InP	50	Cap protection layer
i-InGaAs	145	Absorption layer
i-InGaAs	4	Superlattice layer
i-InAlAs	1	Superlattice layer
i-InGaAs	3	Superlattice layer
i-InAlAs	2	Superlattice layer
i-InGaAs	2	Superlattice layer
i-InAlAs	3	Superlattice layer
i-InGaAs	1	Superlattice layer
i-InAlAs	4	Superlattice layer
i-InAlAs	40	Schottky barrier enhancement layer
i-InP	50	Sacrificial layer
i-InGaAs	200	Etch-stop layer
i-InP	500	Buffer layer
InP substrate	350 (μm)	Substrate
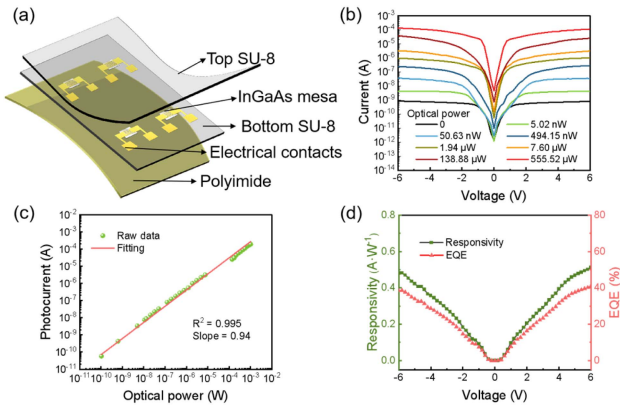
Fig. 2. (a) Laminated structure of flexible InGaAs photodetector; (b) Current-voltage (I-V) curves of InGaAs photodetector in the dark and under illumination with different optical power at 1550 nm; (c) Double logarithm plot of photocurrent versus incident optical power at a bias of 6 V; (d) Responsivity and external quantum efficiency (EQE) under different bias voltages at an optical power of 1.94 μW.

chemical etching. Next, an electrode of 5 nm Ti/100 nm Au was deposited on the InGaAs NM. Following that, the device was encapsulated using SU-8 2005 and photolithography was performed to create metal electrode windows for probe contacts. Finally, the encapsulated device was directly delaminated from the substrate wafer. An optical micrograph of an actual device depicting interdigitated electrodes with a spacing and width of 2 μm is shown in Fig. 1(b).

III. RESULTS AND DISCUSSIONS

The multilayer structure of the flexible InGaAs photodetector is visually displayed in Fig. 2(a). The influence on device performance induced by local stress is negligible through the careful design for the thickness of different cladding layers, in which the main structure for photon-to-electron transition (i.e., InGaAs and metal contact) was subjected to the minimum stress [68]. The static characteristics of flexible InGaAs photodetector were measured by a semiconductor analyzer (PRIMARIUS, FS-Pro). The I-V curves under different optical powers ranging from 0

to 555.52 μW at 1550 nm were demonstrated (Fig. 2(b)), where input optical signal is generated by a tunable semiconductor laser (Santec, TSL-550). The dark current of the photodetector is less than 1 nA, and the on/off ratio is as high as 1.39×10^5 under the optical power of 555.52 μW at 6 V. The nonlinear behavior shown in the I-V curves and the low dark current could be attributed to Schottky contact between InGaAs and metal electrodes. In an MSM photodetector, the dark current is significantly influenced by both the height of the Schottky barrier and the width of the depletion layer [69], [70]. Specifically, the Schottky barrier's height on InGaAs(n^-) is notably low, approximately 0.2 eV [71]. Therefore, direct electrode deposition on the InGaAs absorption layer would result in excessive dark current. This issue can be resolved by employing a layer of thin, undoped, lattice-matched InAlAs layer (with an energy gap of 1.46 eV) [72]. Moreover, it was observed that the photocurrent of the InGaAs photodetector exhibited a linear relationship with the intensity of the optical power. The relationship between photocurrent and optical power was quantified by measuring the photocurrent at a wavelength of 1550 nm and 6 V across a wide optical power range. The resulting data was plotted in Fig. 2(c). Specifically, an erbium-doped fiber amplifier (MChlight, MCEYDFA-HP) and an electronic variable optical attenuator (Thorlabs, V1550A) were employed to control and modulate the incident light power. The InGaAs photodetector exhibited a linear response within the experimental range, which extended from an optical power of 100 pW to 1.02 mW. This indicates a large linear dynamic range (LDR) over 70 dB, which is expected to be one of the largest LDRs among conventional flexible photodetectors [16], [28], [38], [47], [73], [74], [75], [76], [77].

In addition, responsivity and external quantum efficiency (EQE) are two important indicators of performance for a photodetector, as described by the following equations: $R = (I_{ph} - I_d)/P_{in}$ and $EQE = R_\lambda \, hc/q\lambda$, where I_{ph} is the photocurrent, I_d is the dark current, P_{in} is the optical power, h is Planck's constant, c represents the velocity of light in air, q is the electron charge, and λ is the light wavelength. It is shown in Fig. 2(d) that the responsivity at an input power of 1.94 μW was 0.51 A/W, equivalent to an EQE of 41%, which is comparable to that of the rigid counterpart, verifying the reliability and suitability of flexible photodetector fabrication process.

The frequency responses of the flexible InGaAs photodetector were characterized by a vector network analyzer (VNA, Anritsu, MS4647B). The dynamic measurement setup is shown in Fig. 3. An optical modulator (Optilab, LMC-40) was driven by the small signal of the VNA to provide a dynamic optical signal for our photodetector. The DC bias voltage was generated using a digital source meter (Keithley 2450). The results show a 3-dB bandwidth of 2.03 GHz (Fig. 4(a)). The total response time of the photodetector is determined by two factors: the carrier transit time (τ_{tr}) and resistive-capacitive (RC) delay time constant (τ_{RC}). The carrier transit time can be evaluated by $\tau_{tr} = \frac{l^2}{2\mu V_{DS}}$, where l, μ, and V_{DS} are the length of InGaAs photodetector, mobility of InGaAs nanomembrane, and applied bias voltage, respectively. The electron mobility of InGaAs
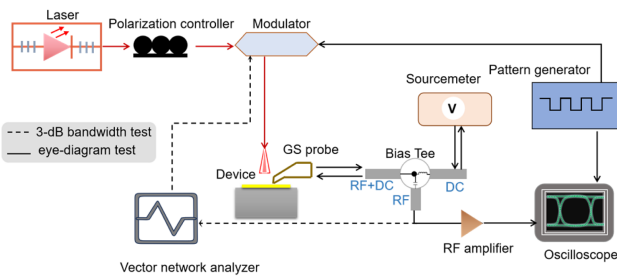
Fig. 3.   Measurement setup for dynamic response characterization, with electrical and optical connections represented by black and red lines, respectively.
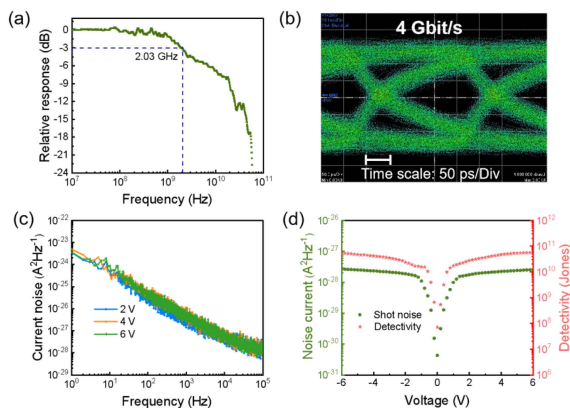

Fig. 4.   (a) Frequency response of flexible InGaAs photodetector; (b) Received eye diagram of OOK signal at a data rate of 4 Gbit/s; (c) 1/f noise spectra of InGaAs photodetector under different voltages; (d) Shot noise and detectivity at different bias voltages.

was measured to be 6.85×10^3 cm^2/(V·s) using the Hall test. When an applied bias is 6 V, the transit-time-limited bandwidth ($f_{tr3dB} = \frac{1}{2\pi\tau_{tr}}$) is calculated to be 327 GHz. However, the measured 3-dB bandwidth is much smaller than the calculated value, thereby suggesting that the overall response time (τ) is determined by τ_{RC}. The RC time constant is calculated by measuring the reflection coefficient S$_{11}$ of the detector using VNA. The resistance of the photodetector (R_{PD}) was determined to be 5.24 Ω, and the device's capacitance was calculated to be 0.51 pF, so the RC-time limited bandwidth($f_{RC3dB} = \frac{1}{2\pi RC}$) ($R = R_{PD} + R_L$, $R_L = 50\ \Omega$) is calculated to be 5.65 GHz. However, accurately predicting the bandwidth of a photodetector based solely on interdigital electrode spacing and RC time constant can be challenging due to the presence of various factors, such as parasitic elements, material properties, and measurement setup considerations. These factors can lead to differences between the predicted and measured bandwidth values. In the future, it will be essential to enhance the design of traveling wave electrodes, specifically for impedance matching to optimize power transfer and minimize reflection. This will enable a larger bandwidth. Additionally, improving the fabrication process is crucial to ensure high- quality absorption and electrode layers, further boosting the bandwidth. Furthermore, we conducted an eye-diagram measurement to showcase the viability of the

InGaAs photodetector in effectively receiving high bit-rate data in optical communication, the 2^{31}-1 PRBS patterned signals are generated by the pules-pattern generator (PPG) (Anritsu, MP2110A), and then amplified by a RF amplifier (Anritsu, AH54147A). Simultaneously, DC bias voltage was generated by the source meter, and then received by a sampling oscilloscope (Anritsu, MP 1900A). The measured eye diagram at 4 Gbit/s at 6 V is shown in Fig. 4(b), and to the best of our knowledge, this is currently the highest speed achieved by a flexible free-space SWIR photodetector. The opening eye diagram proves that our photodetector is expected to be applied in high-speed optical communication.

The noise characteristics refer to the behavior and performance of the photodetector in the presence of various noise sources. To evaluate the noise characteristics of the InGaAs photodetector, we analyzed both 1/f, shot, and thermal noise, in which 1/f noise dominates at low frequency. Hooge's empirical relationship could determine 1/f noise ($S_i = A \cdot i^\alpha / f^\beta$), where i, f, and A are the channel current, the frequency, and noise amplitude, respectively. The measurement results for the 1/f noise are shown in Fig. 4(c), indicating that the noise current decreases from 3.69×10^{-24} A^2·Hz^{-1} at the frequency of 1 Hz to 1.26×10^{-28} A^2·Hz^{-1} at 10^5 Hz at 6 V. Notably, within a specific range, different bias voltages have minimal impact on 1/f noise due to its positive correlation with the current, and the dark current does not exhibit significant changes under these bias voltages. The reduction of 1/f noise can be achieved by decreasing the dark current in the channel. Photodetectors experience a domination of shot and thermal noise when operating at high frequencies. The shot noise was calculated according to $S_S = 2qI_d$, where q, I_d are electron charge and dark current, respectively. Here, we reduced the dark current of the device by increasing the barrier height of the device. The dark current of the InGaAs photodetector is 801 pA at 6 V, and the calculated shot noise is 2.56×10^{-28} A^2·Hz^{-1}. Thermal noise refers to the electronic noise that arises from the thermal motion of charge carriers within an electrical conductor when it is in a state of equilibrium, which could be evaluated by $S_t = 4k_BT/R$, where k_B, T and R were the Boltzmann constant, the temperature (about 300 K in our experiment), and the resistance of the device, respectively. The thermal noise is 2.21×10^{-30} A^2·Hz^{-1} at a bias voltage of 6 V. Therefore, the noise current (i_n) is dominantly determined by shot noise at high frequency. Detectivity is a crucial performance metric for photodetectors, as it quantifies the minimum signal that can be reliably detected, which can be expressed by $D^* = A^{1/2} R/(2qI_d)^{1/2}$, where A represents the effective area of the detector in cm^2, and R is the responsivity in A/W. Our analysis revealed that the flexible photodetector exhibited a room-temperature detectivity of 5.65×10^{10} Jones, primarily limited by shot noise. Moreover, the current noise and detectivity of the device increased with the applied voltage, as shown in Fig. 4(d). This phenomenon can be attributed to two factors: the increased efficiency of the separation-collection process and the enhanced responsivity due to a larger bias voltage source.

Furthermore, we illustrated that the photodetector retains its outstanding optoelectronic performance even when subjected to
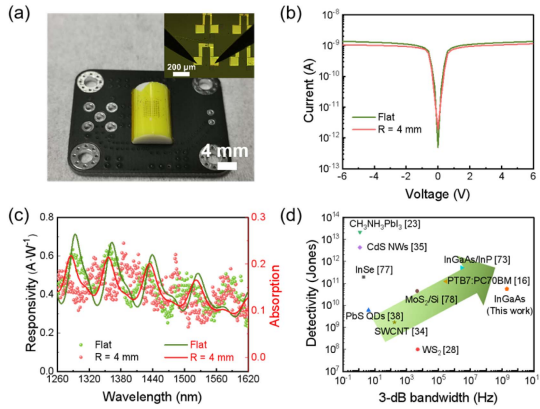
Fig. 5. (a) Photograph of the device attached to a half cylinder with a bend radius of 4 mm. Inset: the top-down view of the device in testing; (b) Dark current of the photodetector in planar and bent states; (c) Experimental spectral response and FDTD simulated absorption spectrum of InGaAs photodetector in planar and bent states; (d) Comparison of performance for some reported flexible free-space photodetectors in terms of 3 dB bandwidth and detectivity. The direction of the green arrow signifies improved performance.

significant mechanical deformation. The device was affixed to a half cylinder with a bend radius of 4 mm, and the signal was conveyed through the probes on the electrode pads (Fig. 5(a)). The dark current and spectral response of the detectors are compared in Fig. 5(b) and (c), for both their nondeformed and bent states. The responsivity of the device is determined by measuring its response to wavelengths spanning approximately 360 nm, which corresponds to the O, E, S, C, and L bands commonly employed in optical communications. The response spectrum displays a sinusoidal jitter, attributed to the interference of multilayer films. Simulating the absorption spectrum using the finite-difference time-domain (FDTD) method has further confirmed this phenomenon. When in the bent state, there is a slight change in the optical absorption spectrum and responsivity curve. This can be attributed to the alterations in the interference effect of the Fabry-Pérot cavity that occurs between the thin films, as a result of the incident light striking the sample surface at an angle. The detector exhibits high responsivity across various wavelengths before and after bending. Fig. 5(d) provides a comparative analysis of the photodetector's performance in relation to currently reported free-space flexible photodetectors [16], [23], [28], [34], [35], [38], [73], [77], [78]. Notably, certain photodetectors utilizing novel materials, such as perovskite, quantum dots, and nanowires, have achieved high impressive detectivity. However, they suffer from limited bandwidth, likely due to inefficient carrier transport and collection [17], [79], [80], [81], [82], [83], [84], [85]. In contrast, the flexible InGaAs photodetector discussed herein demonstrates excellent comprehensive performance for short-wavelength infrared (SWIR) photodetection.

In addition to the optoelectronic and mechanical performance, long-term reliability and stability are crucial factors determining the device's practical feasibility. Therefore, we tested the device's performance with surroundings interference, as shown in Fig. 6. We performed testing on the dark current and photocurrent variations of the photodetector following treatment at temperatures ranging from −30 °C to 100 °C. Each temperature was
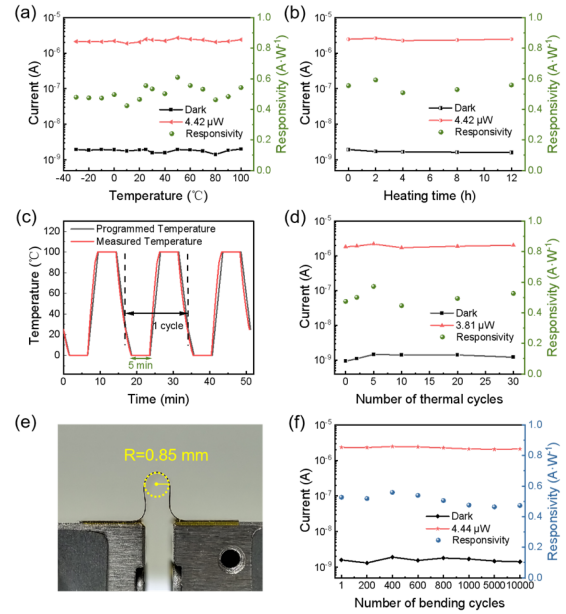

Fig. 6. (a) Dark current, photocurrent, and responsivity of InGaAs photodetector after treatment with different temperatures at 1550 nm; (b) Dark current, photocurrent, and responsivity of the photodetector after being exposed to 50 °C for different time durations; (c) Temperature profile used in thermal cycling tests; (d) Dark current, photocurrent, and responsivity of the photodetector after various thermal cycles. (e) Photo showing the cross-sectional view of the photodetector with a bending radius of 0.85 mm; (f) Dark current, photocurrent, and responsivity of the photodetector after various bending cycles. All tests were performed at a humidity of 43%.

maintained for a duration of 10 minutes (Fig. 6(a)). To assess the durability of the photodetector, we placed it in a 50 °C oven and measured the dark current and photocurrent after insulation for 2 hours, 4 hours, 8 hours, and 12 hours, respectively (Fig. 6(b)). To further verify the stability of the device, a temperature control stage (Zhongqi, TLTP-ZQ5200) was used to cyclically control the temperature between 0–100 °C. The device was cooled from room temperature (25 °C) to 0 °C and kept for 5 minutes, then heated to 100 °C and kept for another 5 minutes, and finally restored to room temperature. This constituted one cycle of thermal cycling (Fig. 6(c)). Thermal cycling tests were performed with different cycles: 2, 5, 10, 20, and 30 (Fig. 6(d)). The nearly unchanged dark current and responsivity of the device indicated that it exhibits excellent stability and durability in complex environments.

The mechanical durability and stability of a flexible photodetector are crucial factors for flexible devices. We assessed the mechanical durability and stability by measuring the retention characteristics of key parameters, including dark current, photocurrent, and responsivity, under varying bending cycles. As shown in Fig. 6(e) and (f), we attached the device to two linear motion stages and adjusted their distance to achieve a bending radius of 0.85 mm for the flexible photodetector. We conducted tests on the dark current and photocurrent and calculated the device's responsivity under various bending cycles. No significant changes in the device's performance were observed during mechanical fatigue tests even after undergoing 10 000 bending cycles, indicating that the detector exhibits impressive

mechanical flexibility and stability. These findings provide evidence for the potential commercialization of the flexible photodetector.

IV. CONCLUSION

In summary, we have demonstrated a flexible InGaAs nanomembrane MSM photodetector on a thin polyimide substrate. The fabrication process involved adhesive-assisted bonding of the epitaxial layers, which were lifted off directly from the parent InP substrate. The photodetector achieved a responsivity of 0.51 A/W, a detectivity of 5.65×10^{10} Jones, and a linear dynamic range exceeding 70 dB. Dynamic measurements show that the 3-dB bandwidth of the photodetector is 2.03 GHz, enabling it to support a data communication rate over 4 Gb/s, which is currently the highest speed achieved by a flexible free-space detector in the SWIR range to the best of our knowledge. Furthermore, the detection range of the photodetector covered the entire telecommunication band, including the O, E, S, C, and L bands. Meanwhile, the optoelectrical performance of the flexible photodetector remained stable even when subjected to a bending state or harsh environmental conditions. These results suggest potential for advanced applications in optical communications, sensing, and wearable devices.

ACKNOWLEDGMENT

REFERENCES

[1] C. H. Kang et al., "High-speed colour-converting photodetector with all-inorganic CsPbBr₃ perovskite nanocrystals for ultraviolet light communication," *Light Sci. Appl.*, vol. 8, no. 1, 2019, Art. no. 94.

[2] Y. Wang et al., "Ultra-compact high-speed polarization division multiplexing optical receiving chip enabled by graphene-on-plasmonic slot waveguide photodetectors," *Adv. Opt. Mater.*, vol. 9, no. 6, 2021, Art. no. 2001215.

[3] J. Zheng et al., "An ultrafast organic photodetector with low dark current for optical communication systems," *ACS Photon.*, vol. 10, pp. 1382–1388, 2023.

[4] N. Flöry et al., "Waveguide-integrated van der Waals heterostructure photodetector at telecom wavelengths with high speed and high responsivity," *Nat. Nanotechnol.*, vol. 15, no. 2, pp. 118–124, 2020.

[5] B. Wang and J. Mu, "High-speed Si-Ge avalanche photodiodes," *PhotoniX*, vol. 3, no. 1, pp. 1–22, 2022.

[6] S. Majumder, T. Mondal, and M. J. Deen, "Wearable sensors for remote health monitoring," *Sensors*, vol. 17, no. 1, 2017, Art. no. 130.

[7] L. Li et al., "Near-infrared light triggered self-powered mechano-optical communication system using wearable photodetector textile," *Adv. Funct. Mater.*, vol. 31, no. 37, 2021, Art. no. 2104782.

[8] N. Matsuhisa et al., "High-frequency and intrinsically stretchable polymer diodes," *Nature*, vol. 600, no. 7888, pp. 246–252, 2021.

[9] L. Li et al., "A fully-integrated flexible photonic platform for chip-to-chip optical interconnects," *J. Light. Technol.*, vol. 31, no. 24, pp. 4080–4086, Dec. 2013.

[10] C. Choi et al., "Flexible optical waveguide film fabrications and optoelectronic devices integration for fully embedded board-level optical interconnects," *J. Light. Technol.*, vol. 22, no. 9, pp. 2168–2176, Sep. 2004.

[11] J. J. Kim et al., "Skin electronics: Next-generation device platform for virtual and augmented reality," *Adv. Funct. Mater.*, vol. 31, no. 39, 2021, Art. no. 2009602.

[12] T. Umezawa, S. Nakajima, A. Matsumoto, K. Akahane, and N. Yamamoto, "Sub-millimeter large high-speed photodetector for FSO communications," in *Proc. Conf. Lasers Electro-Opt.*, San Jose, CA, USA, 2021, pp. 1–2.

[13] L. Lv et al., "Flexible short-wave infrared image sensors enabled by high-performance polymeric photodetectors," *Macromolecules*, vol. 53, no. 23, pp. 10636–10643, 2020.

[14] D. Yu et al., "Broadband and sensitive two-dimensional halide perovskite photodetector for full-spectrum underwater optical communication," *Nano Res.*, vol. 14, pp. 1210–1217, 2021.

[15] Y. Zhu et al., "Skin-like near-Infrared II photodetector with high performance for optical communication, imaging, and proximity sensing," *Chem. Mater.*, vol. 35, no. 5, pp. 2114–2124, 2023.

[16] R. Eckstein et al., "Aerosol-jet printed flexible organic photodiodes: Semitransparent, color neutral, and highly efficient," *Adv. Electron. Mater.*, vol. 1, no. 8, 2015, Art. no. 1500101.

[17] T. N. Ng, W. S. Wong, M. L. Chabinyc, S. Sambandan, and R. A. Street, "Flexible image sensor array with bulk heterojunction organic photodiode," *Appl. Phys. Lett.*, vol. 92, no. 21, pp. 191–320, 2008.

[18] L. Zhang et al., "Self-suspended nanomesh scaffold for ultrafast flexible photodetectors based on organic semiconducting crystals," *Adv. Mater.*, vol. 30, no. 28, 2018, Art. no. 1801181.

[19] D. Yang and D. Ma, "Development of organic semiconductor photodetectors: From mechanism to applications," *Adv. Opt. Mater.*, vol. 7, no. 1, 2019, Art. no. 1800522.

[20] T. Shan, X. Hou, X. Yin, and X. Guo, "Organic photodiodes: Device engineering and applications," *Front. Optoelectron.*, vol. 15, no. 1, 2022, Art. no. 49.

[21] X. Hu, X. Zhang, L. Liang, J. Bao, and Y. Xie, "High-performance flexible broadband photodetector based on organolead halide perovskite," *Adv. Funct. Mater.*, vol. 24, no. 46, pp. 7373–7380, 2014.

[22] S. Chen et al., "A flexible UV-vis-NIR photodetector based on a perovskite/conjugated-polymer composite," *Adv. Mater.*, vol. 28, no. 28, pp. 5969–5974, 2016.

[23] H. Sun, W. Tian, F. Cao, J. Xiong, and L. Li, "Ultrahigh-performance self-powered flexible double-twisted fibrous broadband perovskite photodetector," *Adv. Mater.*, vol. 30, no. 21, 2018, Art. no. 1706986.

[24] D. H. Chun et al., "Nanopatterning on mixed halide perovskites for promoting photocurrent generation of flexible photodetector," *Adv. Funct. Mater.*, vol. 32, no. 43, 2022, Art. no. 2206995.

[25] M. Tan et al., "Carbonized polymer dots enhanced stability and flexibility of quasi-2D perovskite photodetector," *Light Sci. Appl.*, vol. 11, no. 1, 2022, Art. no. 304.

[26] B. Jin et al., "Self-limited epitaxial growth of ultrathin nonlayered CdS flakes for high-performance photodetectors," *Adv. Funct. Mater.*, vol. 28, no. 20, 2018, Art. no. 1800181.

[27] S. Pak et al., "Strain-engineering of contact energy barriers and photoresponse behaviors in monolayer MoS₂ flexible devices," *Adv. Funct. Mater.*, vol. 30, no. 43, 2020, Art. no. 2002023.

[28] J. Quereda et al., "Scalable and low-cost fabrication of flexible WS₂ photodetectors on polycarbonate," *npj Flex. Electron.*, vol. 6, no. 1, 2022, Art. no. 23.

[29] Y. Zou et al., "High-temperature flexible WSe₂ photodetectors with ultrahigh photoresponsivity," *Nat. Commun.*, vol. 13, no. 1, 2022, Art. no. 4372.

[30] D. Zhang et al., "Flexible computational photodetectors for self-powered activity sensing," *npj Flex. Electron.*, vol. 6, no. 1, 2022, Art. no. 7.

[31] L. Kong et al., "Inkjet-printed, large-area, flexible photodetector array based on electrochemical exfoliated MoS₂ film for photoimaging," *Adv. Eng. Mater.*, vol. 25, no. 2, 2023, Art. no. 2200946.

[32] G. Yu, Z. Liu, X. Xie, X. Ouyang, and G. Shen, "Flexible photodetectors with single-crystalline GaTe nanowires," *J. Mater. Chem. C*, vol. 2, no. 30, pp. 6104–6110, 2014.

[33] X. Xuming and S. Guozhen, "Single-crystalline In₂S₃ nanowire-based flexible visible-light photodetectors with an ultra-high photoresponse," *Nanoscale*, vol. 7, no. 11, pp. 5046–5052, 2015.

[34] S. Park et al., "Significant enhancement of infrared photodetector sensitivity using a semiconducting single-walled carbon nanotube/C₆₀ phototransistor," *Adv. Mater.*, vol. 27, no. 4, pp. 759–765, 2015.

[35] L. Li, Z. Lou, and G. Shen, "Hierarchical CdS nanowires based rigid and flexible photodetectors with ultrahigh sensitivity," *ACS Appl. Mater. Interfaces*, vol. 7, no. 42, pp. 23507–23514, 2015.

[36] Z. Zheng, L. Gan, J. Zhang, F. Zhuge, and T. Zhai, "An enhanced UV–Vis–NIR an d flexible photodetector based on electrospun ZnO nanowire array/PbS quantum dots film heterostructure," *Adv. Sci.*, vol. 4, no. 3, 2017, Art. no. 1600316.

[37] J. He et al., "Synergetic effect of silver nanocrystals applied in PbS colloidal quantum dots for high-performance infrared photodetectors," *Acs Photon.*, vol. 1, no. 10, pp. 936–943, 2014.

[38] T.-H. Kim et al., "Fully stretchable optoelectronic sensors based on colloidal quantum dots for sensing photoplethysmographic signals," *Acs Nano*, vol. 11, no. 6, pp. 5992–6003, 2017.

[39] Z. Ren et al., "Bilayer PbS quantum dots for high-performance photodetectors," *Adv. Mater.*, vol. 29, no. 33, 2017, Art. no. 1702055.

[40] T. Shen, D. Binks, J. Yuan, G. Cao, and J. Tian, "Enhanced-performance of self-powered flexible quantum dot photodetectors by a double hole transport layer structure," *Nanoscale*, vol. 11, no. 19, pp. 9626–9632, 2019.

[41] K. Shen et al., "Flexible and self-powered photodetector arrays based on all-inorganic CsPbBr$_3$ quantum dots," *Adv. Mater.*, vol. 32, no. 22, 2020, Art. no. 2000004.

[42] M. H. Tran and J. Hur, "Direct, simple, rapid, and real-time monitoring of ultraviolet B level in sunlight using a self-powered and flexible photodetector," *EcoMat*, vol. 5, no. 3, 2023, Art. no. e12301.

[43] D. Fan, K. Lee, and S. R. Forrest, "Flexible thin-film InGaAs photodiode focal plane array," *Acs Photon.*, vol. 3, no. 4, 2016, pp. 670–676.

[44] M. Cho, J. H. Seo, M. Kim, J. Lee, and Z. Ma, "Resonant cavity germanium photodetector via stacked single-crystalline nanomembranes," *J. Vac. Sci. Technol. B*, vol. 34, no. 4, 2016.

[45] M. Kim, J. H. Seo, Z. Yu, W. Zhou, and Z. Ma, "Flexible germanium nanomembrane metal-semiconductor-metal photodiodes," *Appl. Phys. Lett.*, vol. 109, no. 5, 2016, Art. no. 051105.

[46] H. Zhang, T.-H. Chang, S. Min, and Z. Ma, "Flexible semiconductor Device Technologies," in *Proc. IEEE 5th Electron Devices Technol. Manuf. Conf.*, Chengdu, China, 2021, pp. 1–3.

[47] S. An et al., "High-sensitivity and mechanically compliant flexible Ge photodetectors with a vertical p–i–n configuration," *ACS Appl. Electron. Mater.*, vol. 3, no. 4, pp. 1780–1786, 2021.

[48] W. Yang et al., "Large-area InP-based crystalline nanomembrane flexible photodetectors," *Appl. Phys. Lett.*, vol. 96, no. 12, 2010, Art. no. 121107.

[49] L. Menon et al., "Transferred flexible three-color silicon membrane photodetector arrays," *IEEE Photon. J.*, vol. 7, no. 1, Feb. 2015, Art. no. 6800106.

[50] J. H. Seo, Z. Kan, M. Kim, D. Zhao, and Z. Ma, "High performance flexible phototransistors based on transferrable silicon nanomembranes," in *Proc. Prog. Electromagn. Res. Symp.*, 2016, pp. 2406–2407.

[51] M. Kim, J. H. Seo, Z. Yu, W. Zhou, and Z. Ma, "Flexible germanium nanomembrane metal-semiconductor-metal photodiodes," *Appl. Phys. Lett.*, vol. 109, no. 5, pp. 527–534, 2016.

[52] G. Qin, H. C. Yuan, Y. Qin, J. H. Seo, and Z. Ma, "Fabrication and characterization of flexible microwave single-crystal germanium nanomembrane diodes on a plastic substrate," *IEEE Electron Device Lett.*, vol. 34, no. 2, pp. 160–162, Feb. 2013.

[53] M. Kim et al., "Light absorption enhancement in Ge nanomembrane and its optoelectronic application," *Opt. Exp.*, vol. 24, no. 15, 2016, Art. no. 16894.

[54] S. Adachi, *Physical Properties of III-V Semiconductor Compounds*. Hoboken, NJ, USA: John Wiley & Sons, 1992.

[55] J. Bowers and C. Burrus, "Ultrawide-band long-wavelength pin photodetectors," *J. Light. Technol.*, vol. 5, no. 10, pp. 1339–1350, Oct. 1987.

[56] H. Xu et al., "Flexible organic/inorganic hybrid near-infrared photoplethysmogram sensor for cardiovascular monitoring," *Adv. Mater.*, vol. 29, no. 31, 2017, Art. no. 1700975.

[57] L. Yang et al., "Low-cost copper electrode for high-performance panchromatic multiplication-type organic photodetectors with optical microcavity effect," *Adv. Funct. Mater.*, vol. 32, no. 20, 2022, Art. no. 2108839.

[58] J. An et al., "Single-step selective laser writing of flexible photodetectors for wearable optoelectronics," *Adv. Sci.*, vol. 5, no. 8, 2018, Art. no. 1800496.

[59] X. C. Tan et al., "Skin-mimicking, stretchable photodetector for Skin-customized ultraviolet dosimetry," *Adv. Mater. Technol.*, vol. 7, no. 8, 2022, Art. no. 2101348.

[60] H. C. Ko et al., "A hemispherical electronic eye camera based on compressible silicon optoelectronics," *Nature*, vol. 454, no. 7205, pp. 748–753, 2008.

[61] I. Jung et al., "Dynamically tunable hemispherical electronic eye camera system with adjustable zoom capability," *Proc. Nat. Acad. Sci.*, vol. 108, no. 5, pp. 1788–1793, 2011.

[62] Y. M. Song et al., "Digital cameras with designs inspired by the arthropod eye," *Nature*, vol. 497, no. 7447, pp. 95–99, 2013.

[63] C. Choi et al., "Human eye-inspired soft optoelectronic device using high-density MoS$_2$-graphene curved image sensor array," *Nature Commun.*, vol. 8, no. 1, 2017, Art. no. 1664.

[64] L. Gu et al., "A biomimetic eye with a hemispherical perovskite nanowire array retina," *Nature*, vol. 581, no. 7808, pp. 278–282, 2020.

[65] N. Strobel et al., "Color-selective printed organic photodiodes for filterless multichannel visible light communication," *Adv. Mater.*, vol. 32, no. 12, 2020, Art. no. 1908258.

[66] M. Rein et al., "Diode fibres for fabric-based optical communications," *Nature*, vol. 560, no. 7717, pp. 214–218, 2018.

[67] L. Li et al., "High-performance flexible waveguide-integrated photodetectors," *Optica*, vol. 5, no. 1, pp. 44–51, 2018.

[68] L. Lan et al., "Integrated flexible chalcogenide glass photonic devices," *Nat. Photon.*, vol. 8, no. 8, pp. 643–649, 2014.

[69] G. Dastgeer et al., "Temperature-dependent and gate-tunable rectification in a black phosphorus/WS$_2$ van der Waals heterojunction diode," *ACS Appl. Mater. Interfaces*, vol. 10, no. 15, pp. 13150–13157, 2018.

[70] S. Shafique et al., "Improving the performance of V$_2$O$_5$/rGO hybrid nanocomposites for photodetector applications," *Sens. Actuators, A*, vol. 332, 2021, Art. no. 113073.

[71] J. B. Soole and H. Schumacher, "InGaAs metal-semiconductor-metal photodetectors for long wavelength optical communications," *IEEE J. Quantum Electron.*, vol. 27, no. 3, pp. 737–752, Mar. 1991.

[72] E. Sano, M. Yoneyama, T. Enoki, and T. Tamamura, "Performance dependence of InGaAs MSM photodetectors on barrier-enhancement layer structures," *Electron. Lett.*, vol. 13, no. 28, pp. 1220–1221, 1992.

[73] X. Li et al., "High performance visible-SWIR flexible photodetector based on large-area InGaAs/InP PIN structure," *Sci. Rep.*, vol. 12, no. 1, 2022, Art. no. 7681.

[74] S. Park et al., "Ultraflexible near-infrared organic photodetectors for conformal photoplethysmogram sensors," *Adv. Mater.*, vol. 30, no. 34, 2018, Art. no. 1802359.

[75] H. Jing et al., "Flexible ultrathin single-crystalline perovskite photodetector," *Nano Lett.*, vol. 20, no. 10, pp. 7144–7151, 2020.

[76] W. Wu et al., "Flexible photodetector arrays based on patterned CH$_3$NH$_3$PbI$_{3-x}$Cl$_x$ perovskite film for real-time photosensing and imaging," *Adv. Mater.*, vol. 31, no. 3, 2019, Art. no. 1805913.

[77] P. Li et al., "Flexible photodetectors based on all-solution-processed Cu electrodes and InSe nanoflakes with high stabilities," *Adv. Funct. Mater.*, vol. 32, no. 10, 2022, Art. no. 2108261.

[78] J.-M. Choi et al., "Ultra-flexible and rollable 2D-MoS$_2$/Si heterojunction-based near-infrared photodetector via direct synthesis," *Nanoscale*, vol. 13, no. 2, pp. 672–680, 2021.

[79] Z. Li, G. Lakhwani, N. C. Greenham, and C. R. McNeill, "Voltage-dependent photocurrent transients of PTB7: PC70BM solar cells: Experiment and numerical simulation," *J. Appl. Phys.*, vol. 114, no. 3, 2013.

[80] M. Wang et al., "High open circuit voltage in regioregular narrow band gap polymer solar cells," *J. Amer. Chem. Soc.*, vol. 136, no. 36, pp. 12576–12579, 2014.

[81] J. Ma and L.-W. Wang, "The nature of electron mobility in hybrid perovskite CH$_3$NH$_3$PbI$_3$," *Nano Lett.*, vol. 17, no. 6, pp. 3646–3654, 2017.

[82] A. S. Aji, P. Solís-Fernández, H. G. Ji, K. Fukuda, and H. Ago, "High mobility WS$_{Fig}$ transistors realized by multilayer graphene electrodes and application to high responsivity flexible photodetectors," *Adv. Funct. Mater.*, vol. 27, no. 47, 2017, Art. no. 1703448.

[83] W. Li, S. Poncé, and F. Giustino, "Dimensional crossover in the carrier mobility of two-dimensional semiconductors: The case of InSe," *Nano Lett.*, vol. 19, no. 3, pp. 1774–1781, 2019.

[84] R. Ma, X. Wei, L. Dai, H. Huo, and G. Qin, "Synthesis of CdS nanowire networks and their optical and electrical properties," *Nanotechnology*, vol. 18, no. 20, 2007, Art. no. 205605.

[85] L. Hu, S. Huang, R. Patterson, and J. E. Halpert, "Enhanced mobility in PbS quantum dot films via PbSe quantum dot mixing for optoelectronic applications," *J. Mater. Chem. C*, vol. 7, no. 15, pp. 4497–4502, 2019.

Yuting Ye received the B.E. degree in materials science and engineering from Zhejiang Sci-Tech University, Hangzhou, China, in 2015, and the M.E. degree in materials engineering from Zhejiang University, Hangzhou, China, in 2018. She is currently working toward the Ph.D. degree in electronic science and technology with Westlake University, Hangzhou, China. Her research interests include flexible photodetector arrays and high-performance imaging sensors.

Hui Ma received the B.E. degree from Central South University, Changsha, China, in 2019. He is currently working toward the Ph.D. degree in electronic science and technology with Zhejiang University, Hangzhou, China. His research focuses on mid-infrared waveguide integrated photodetector.

Jianghong Wu received the B.E. degree in electronic science and technology from the Ningbo University of Technology, Ningbo, China, in 2016, and the M.E. and Ph.D. degree in electronic science and technology from Zhejiang University, Hangzhou, China, in 2019 and 2023, respectively. He is currently a Postdoctoral Associate with The Hong Kong Polytechnic University, Hong Kong. His research interests include waveguide-integrated photodetectors and modulators.

Boshu Sun received the B.E. degree from the Beijing University of Technology, Beijing, China, in 2018, and the M.E. degree from the University of Delaware, Newark, DE, USA, in 2021. She is currently working toward the Ph.D. degree in electronic science and technology with Westlake University, Hangzhou, China. Her research interests include integrated optical sensing and silicon photonics.

Jialing Jian received the B.E. degree in electronic science and technology from Shenzhen University, Shezhen, China, in 2016, and the M.E. degree in optical engineering from the Beijing University of Technology, Beijing, China, in 2020. She is currently working toward the Ph.D. degree in electronic science and technology with Westlake University, Hangzhou, China. Her research focuses on high-speed plasmonic-slicon hybrid integrated optoelectronic device.

Maoliang Wei received the B.E. degree from Xiamen University, Xiamen, China, in 2019. He is currently working toward the Ph.D. degree in electronic science and technology with Zhejiang University, Hangzhou, China. His research focuses on integrated optical computing based on phase change material.

Renjie Tang received the B.E. degree in electronic science and technology from East China Normal University, Shanghai, China, in 2020. He is currently working toward the Ph.D. degree in electronic science and technology with Westlake University, Hangzhou, China. His research focuses on the cavity design and fabrication of on-chip light sources based on solution-processed gain materials.

Yilin Shi received the B.E. degree in electronic science and technology from Heilongjiang University, Heilongjiang, China, in 2020. He is currently working toward the Ph.D. degree in electronic science and technology with Westlake University, Hangzhou, China. His research focuses on the design and fabrication of metasurface devices based on flexible substrates.

Hongtao Lin (Member, IEEE) received the B.S. degree in materials science and engineering from the University of Science and Technology of China, Hefei, China, in 2010, and the Ph.D. degree in materials science and engineering from the University of Delaware, Newark, DE, USA, in 2015. Since 2015, he has been a Postdoctoral Associate with the Massachusetts Institute of Technology, Cambridge, MA, USA, for three years. In 2018, he joined Zhejiang University, Hangzhou, China, as an Assistant Professor. His research interests include medium wave infrared optoelectronics integration and its applications in the fields of on-chip spectrometers, transceiver systems and LiDAR, low dimensional materials optoelectronic integration and extreme light field control and device applications to build future optoelectronic systems, near zero power OFPGA – Applications: optical computing, quantum computing, microwave photons; metasurface - spectrometers, thermal imaging, and microsystems.

Lan Li (Member, IEEE) received the B. S. degree in materials science and engineering from the University of Science and Technology of China, Hefei, China, in 2010, and the Ph.D. degree in materials science and engineering from the University of Delaware, Newark, DE, USA, in 2016. Since 2016, she has been a Postdoctoral Associate with the Massachusetts Institute of Technology, Cambridge, MA, USA, for three years. In 2019, she joined Westlake University, Hangzhou, China, as an Assistant Professor. Her research interests include nanophotonic materials and devices, infrared optical glass materials, integrated flexible photonic device fabrication, characterization, and applications.